SPE Paper Number 95685

Waterflood Surveillance and Control: Incorporating Hall Plot and Slope Analysis

D. B. Silin, SPE, Lawrence Berkeley National Laboratory and University of California, Berkeley; R. Holtzman, University of California, Berkeley; T. W. Patzek, SPE, University of California, Berkeley; J. L. Brink, SPE, Chevron North America Exploration and Production Company; M. L. Minner, Chevron North America Exploration and Production Company

Abstract

Waterflood automation at a field scale is a complex coupled problem. In our analysis, data from injecting and producing wells, as well as satellite differential interferograms (InSAR) are used as the inputs. Some information processing is carried out on-line automatically, and other needs personnel expertise. Dynamic adaptive control is performed in the mixed open-loop-feedback mode. Our surveillance-control system is being implemented in Sections 32 and 33 of the Lost Hills diatomite field, CA, USA.

Introduction

Automation of waterflood surveillance and control helps to make oil recovery operations more efficient and reduce the costs related to early water breakthrough and well failure. Early warnings about possible trouble spots help to make corrective actions in a timely manner. Automation is an attractive, but challenging task[1]. Automated data acquisition and storage technologies have made impressive advances over the past decade[2]. However, it is insufficient to only collect and store the exponentially growing volumes of often meaningless data. The focus should be shifted to the development of robust on-line data analysis and quality control. In waterflood operations, this analysis should result in injection set points that can be sent to the wellhead controllers to close the control loop.

The paper is organized as follows. First, the principles of dynamic adaptive control are discussed. Then, several on-line and off-line methods of monitoring performance of an injection well are reviewed and evaluated. After that, examples of simultaneous analysis of the InSAR subsidence maps[3] and maps based on performance analysis of the individual wells in the project are presented. Two Appendices include brief background material related to the Hall plot, slope analysis, and the frequency-domain asymptotic estimates of time-dependent formation properties.

Dynamic adaptive control

Waterflood projects affect reservoir dynamics over large portions of oilfields. However, oil is produced and water is injected locally through individual wells. Therefore, it is natural to control an entire waterflood project by adjusting injection rates and pressures individually at each well. Clearly, the injection rates and pressures are coupled parameters: An increasing injection pressure results in an increased rate, and *vice versa*. In a moving car, the driver adjusts the accelerator pedal to increase or decrease the torque passed from the engine to the wheels to maintain the desired speed. Similarly, the force driving a waterflood, the injection pressure, is regulated to maintain the desired injection rate. In a car, the engine power is regulated by opening and closing a fuel throttle. At a well, the pressure is regulated by a valve installed at the wellhead. Therefore, the objective of the control at each individual well is to set up the pressure in such a way that the injection rate is maintained at the desired level. How to select the target rates for each well depends on an analysis of performance of a group of wells or the entire field. This analysis includes oil, water, and gas rates at producing wells, subsidence and consequent well failure, rock mechanics and physics, oil prices, *etc*. Below, a subsidence case is analyzed using satellite InSAR images[a], see also Ref. 3.

The formation conditions near the wellbore change in the course of operations. Especially, this is the case when the reservoir rock is low-permeability, soft, and prone to damage, like the diatomite[4,5]. The injection pressure must be adjusted according to these changing conditions; therefore, control must be dynamic. There are two major types of regulation: open-loop and closed-loop control. The former means that the control set points are planned in advance for a substantial period of time, whereas the latter one means that the set points are generated from the current measurements of available parameters. In fact, for injection control, neither of these two modes is suitable in its pure form. The open-loop control requires a reliable model of the process with accurately specified parameters that are almost never available for subsurface fluid flow. The closed-loop control or, otherwise, the feedback regulator, is also not suitable because the current injection conditions are the result of the history of well

---

[a] InSAR images are produced by Vexcel Corporation.

operations, Refs. [6,7]. Therefore, a mixed control scheme has been selected, see **Fig. 1**. The set points are generated in cycles: At the end of each cycle, the model and the target rates are updated, and new set points are computed based on this updated information.

For an injection well, the main parameters usually are the injection rate and pressure. Certainly, the fluid properties are of great importance. For an injection well these properties usually do not vary significantly in time and can be assumed constant over the time of operations (unless of course the water salt and solid content, as well as bacteria counts change considerably). The set point is computed based on the target injection rate and analysis of the near-wellbore reservoir conditions. For the latter task, the injection pressure and rate are extracted from the continuously updated database over a period of time. These data are processed to optimally generate a set point. Here optimality means maintenance of the target injection rate. The target injection rate is external to the well control scheme in Fig. 1. It has to be developed from an analysis of field operations over one or several patterns.
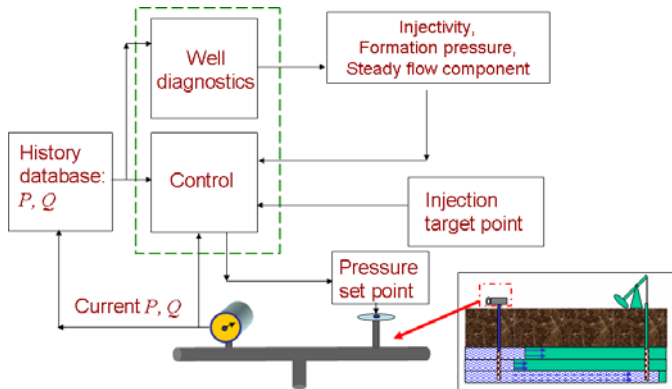

Fig. 1. Individual well control schematic: the data, injection pressures and rates are periodically measured and stored in a database. The set point is generated based on analysis of both the current and historic data.

Once the necessary calculations have been carried out, a pressure set point is generated and passed to the wellhead valve controller. Thus, the control scheme Fig. 1 operates in its own time cycles: the current set point is applied for a period of time until a new set point for the next cycle is generated. Our data processing algorithm for optimal set point generation uses a model of fluid flow in the vicinity of the wellbore. Such a model should be adequate for the type of the well. For instance, the models of flow near hydrofractured and not hydrofractured wells are different. The good news, though, is that the steady-state for radial and non-radial flow models leads to the similar relationships between injection rates and pressures at the wellbore[8]. In any case, identification of parameters based on these models involves a significant degree of uncertainty. Therefore, there is little or no chance to estimate the well injectivity only once and then use this value in the pressure point generation. Even a very good-fit history match cannot yet provide the estimated parameters with long-time predictive capabilities. Therefore, the model parameters must be re-identified during each control cycle. This periodical re-identification of model parameters makes the control scheme *adaptive*.

The parameter identification procedure mentioned above must meet several requirements. It should be model-based, simple, robust, and must not require an interruption of regular field operations. The requirements of this "wish list" are almost contradictory to each other. Conventional transient well-test analysis methods[9,10] require special operations at the well, often including its shut-in. Although recently methods have been developed to perform transient well test analysis on regular operations data[11,12], a careful selection of an appropriate data interval may be needed, and it is impossible to make such a selection blindly in automatic mode. Attempts to separate steady-state and transient components of a flow, see Refs. 13, 6 and 7, show that regular water injection operations are dominated by quasi-steady-state flow. In other words, the transient effects are pronounced only over a time scale much longer than a reasonable time scale of control cycling, or when the injection parameters fluctuate near their steady-state values. Thus, transient well data analysis methods can be used on-line only and are not suitable for automated injection data analysis.

A simple and efficient method of injection well performance monitoring at steady-state flow has been proposed by Hall[14] in 1961. Silin *et al.*[15] reviewed some uncertainties associated with this method and proposed to partially resolve them using a novel "slope analysis." The idea of using Hall's method in automatic maintenance of a desired target injection rate is similar to that of using a thermostat for maintaining a constant temperature. If the rate over a control cycle exceeds or is below the target rate, then the pressure should be increased or decreased, respectively. The Hall plot method is an efficient means of computation of the appropriate injection pressure corrections. In the next section, we consider some technical aspects of the proposed procedure in more detail.

On-line and off-line well monitoring and diagnostics
The argument in the previous section suggests that injection well monitoring and control should be performed by a combination of on-line automatic procedures and off-line analysis requiring input from reservoir engineers. In the following subsections, we briefly describe the automated on-line procedure and present samples of the off-line analysis.

Automatic pressure set point generation using the Hall plot and slope analyses
The Hall plot analysis (see Appendix A), due to its simplicity, can be used efficiently for the on-line injection pressure set point calculation. Once the data over the last control cycle have been acquired, the Hall plot can be used to update the model and to calculate the pressure set point. For example, **Fig. 2** displays a 2-day interval of injection data from a well. Using Hall's analysis, the proportionality coefficient between the integral of injection pressure and cumulative injection (see Eqs. (5) and (6)) is estimated. This proportionality coefficient must be equal to the coefficient of the injection rate Q in Eq. (4). For example, using a well injecting 200 bbl/day, substitution of the estimated coefficient and the target rate of 200 bbl/day back into Eq. (4) yields the pressure set point 1041 psi. This value does not differ much

from the average pressures over the considered time interval, which is an indication of stable injection.

The Hall plot in **Fig. 3**, has been corrected using the slope analysis described in Appendix A, see also Ref. 15.. After this correction, the Hall plot shows a tiny increase of the slope, which means a decrease of injectivity at the beginning of the data interval. Apparently, this behavior might be related to the irregular injection pressure during the first half-day of water injection displayed in Fig. 2.

The computed pressure set point is applied on the next control cycle, after which the computations are repeated and the set point is refreshed.
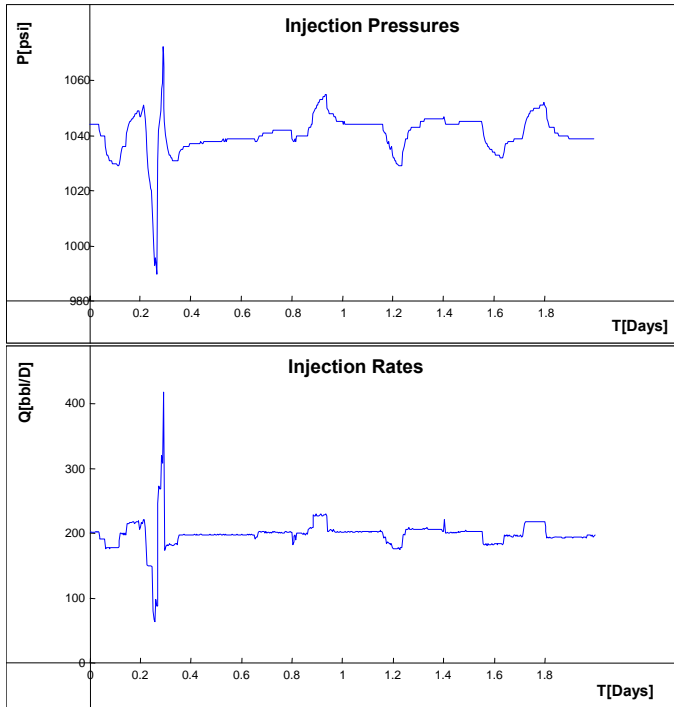

Fig. 2. Injection pressure [psi] and injection rate [bbl/day], both measured every 5 minutes, versus time in days.
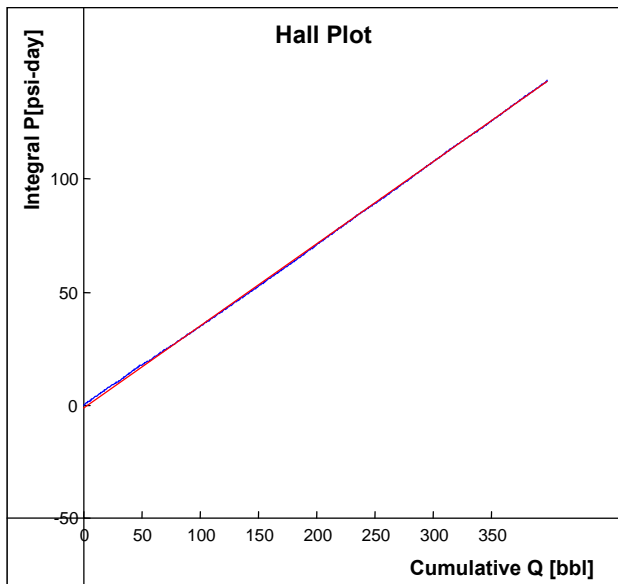

Fig. 3. The Hall plot analysis of the data from Fig. 2. The blue curve is the data and the fitting straight line is red. There is a tiny slope decrease between 0 and 100 bbl of cumulative injection.

The described procedure requires very simple computations, which can be conducted in a fraction of a second on a low-performance computer. Since the pressure set point is periodically refreshed on every control cycle, the procedure is dynamic. It handles the uncertainties associated with the injection zone characterization by fitting the continuously acquired data over each control cycle, so that the current model is applied to the next cycle only and updated afterwards. This feature makes the control adaptive. As an additional safeguard preventing unwanted formation damage, the injection pressure increment between two consecutive cycles can be limited. Such a constraint makes steady-state performance of each injection well stable. However, a different procedure may be required when the well is started or shut-in, if the admissible increment is conservatively small.

Combining slope analysis with transient analysis

The data presented in Fig. 2 also show several intervals of transient pressure and rate behavior. This circumstance makes applicable transient well test analysis methods. Refs. 11 and 12 have developed a method for analysis of regular injection data. This method accounts for the fact that regular operations data are the result of superposition of the steady-state pressure distribution developed near the wellbore and the transient fluctuations. The injection rate corresponding to this distribution is an additional fitting parameter.
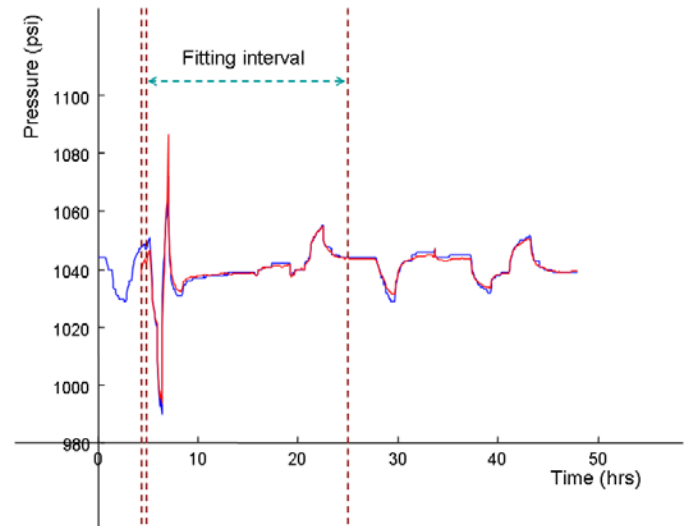

Fig. 4. Transient well test analysis of the data in Fig. 2. The data (blue curve) are fitted on the time interval between the two rightmost vertical dashed lines. The fitting curve (red) is extended to the right beyond the fitting interval based on the fitting results. Thus obtained prediction curve follows the data quite accurately.

Such analysis has been applied to the data from Fig. 2 using the numerical code ODA, see Ref. 11. The result of the fitting is presented in **Fig. 4**. The numerical results are: the transmissivity of 0.6 D-ft/cp, and the reservoir pressure of about 843 psi. In comparison, the slope analysis produced 971 psi. The slope analysis of the data in Fig. 2 yields reservoir pressure at a distance where the pressure fluctuations become negligible at the time scale of the fluctuations of the data. This distance and the reservoir pressure estimate are coupled with each other, see Appendix B.

If, in addition to random fluctuations, *prescribed* fluctuations are imposed by the valve control, then the slope analysis results from different wells can be standardized and a map of the estimated reservoir pressures be drawn. An example of the slope-analysis pressure estimates is presented in **Fig. 8** and **Fig. 9**. Note that the slope and intercept maps have a close correspondence with the short and long-string surface injection pressures in **Fig. 10** and **Fig. 11**. The latter two maps have been obtained only for wells injecting at similar rates.

Formation properties analysis using periodic fluctuations

The formation properties can be estimated by using frequency-domain analysis, see e.g., Ref. 22. It is somewhat similar to pulse-test analysis, which is described in the literature, see Refs. 16, 17, 18. In fact, special periodic fluctuations may not be needed because a time series can be represented as a trigonometric sum or Fourier integral. In other words, these time series can be processed using Fourier transform. It is demonstrated in Appendix B that the Fourier transform of the pressure diffusion equation (8) is asymptotically equivalent to the Fourier transform of the steady-state solution (4) evaluated at the wellbore. It is also shown that the asymptotic requirements are satisfied within a reasonably broad range of reservoir properties and frequencies. Hence, one can treat the injection rate and pressure in Equations (4) as time series and numerically evaluate their amplitudes at different frequencies using, *e.g.*, the fast Fourier transform, see *e.g.* Ref. 19. Since the amplitude of a constant is zero at any non-zero frequency, the ratio of the pressure and rate amplitudes should provide an estimate of the coefficient $\dfrac{\mu}{2\pi kH}\ln\dfrac{r_e(\omega)}{r_w}$, which is the reciprocal of the injectivity index, Ref. 9. The amplitudes of fluctuations determine the data-to-noise ratio. If injection goes "too smoothly," and the rates and pressures are practically constant, no information about the injectivity index can be extracted. However, if the injection rate and pressure are fluctuated near some reference values with a prescribed periodicity, both the slope analysis and the frequency-domain analysis can produce valuable information about the injection well and reservoir performance. The amplitude of such fluctuations does not need to be large, so no interruption of regular operations is required.

The current analysis is complicated by the dependence of the external influence zone radius on the frequency. A similar difficulty is discussed in Appendix A with regard to the slope analysis. To inspect the dependence of the influence zone radius r_e on the frequency, synthetic data were generated and analyzed. The model of superposition of transient and steady flows used in the transmissivity estimates in Refs.11 and 12 was used to generate time series corresponding to the piecewise-constant periodic injection rates. The real data fitting results, Fig. 4, were used as the input parameters. The model simplicity allows us to do most computations semi-analytically. An example of the generated data is displayed in **Fig. 5**. The rates and pressures are sampled every 5 minutes. Periodic data are very suitable for frequency-domain analysis

because the main frequency is known and does not need to be detected using Fourier analysis.
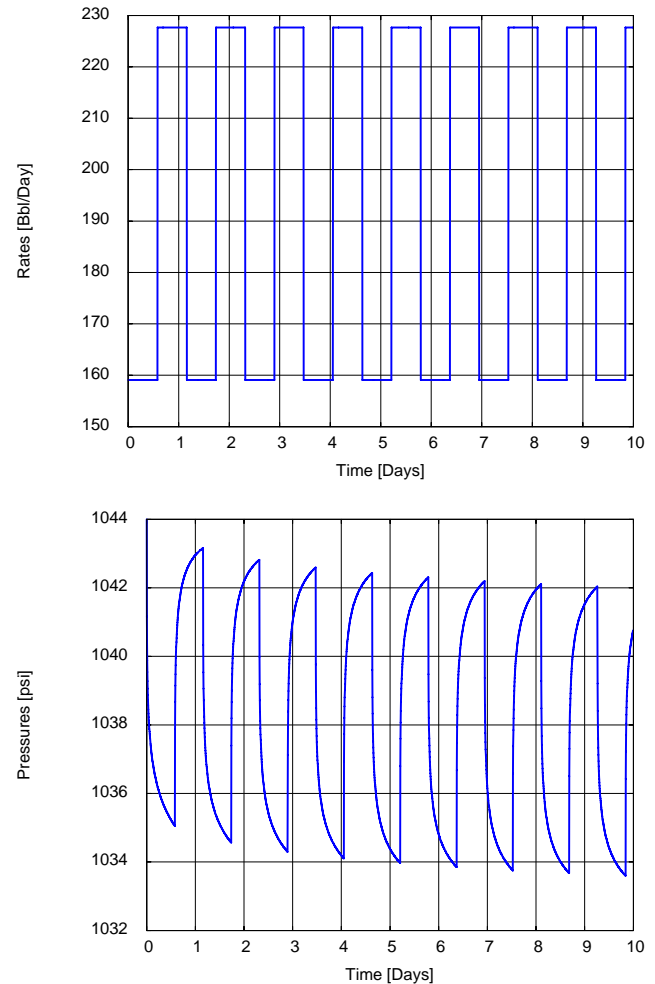

Fig. 5. The synthetic injection rate-injection pressure data oscillates at 10^{-5} Hz.

To investigate the influence of the frequency on the injectivity index and, thereby, on the influence zone radius, a series of data sets has been generated at the same formation properties but varying frequencies of the fluctuations. Plotting $\ln(r_e(\omega)/r_w)$ versus the logarithm of frequency, one obtains a linear dependence, which suggests a power law dependence of the radius of influence on the frequency. The power exponent is different from the expected square root of frequency decay. The reason may be in the fact that the data are not ideal periodic functions, but a time series spanning a finite interval. This, in particular, is the reason of the presence of a decaying trend in the pressures plot in Fig. 5.

To test the dependence of the radius of the influence zone on the permeability, the same model was used to generate a series of data sets at a fixed frequency, but with a variable transmissivity coefficient. We assume that the transmissivity coefficient variations are exclusively due to the permeability variations, while all other parameters remain unchanged. The results of these simulations are plotted in the semilog coordinates in **Fig. 7**. Again, the decay is scaled as a power of the transmissivity, but the exponent is different from one half.

The reason is apparently the same: the data are not ideally periodic time series.
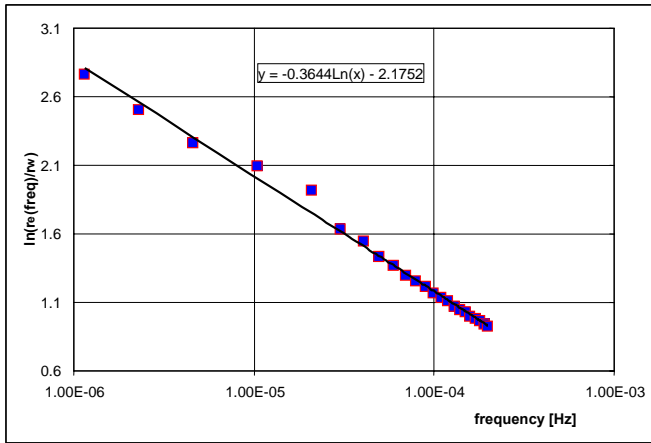

Fig. 6. $r_e(\omega)$ **decays as a power function of the frequency. The decay exponent is different from the expected square root.**
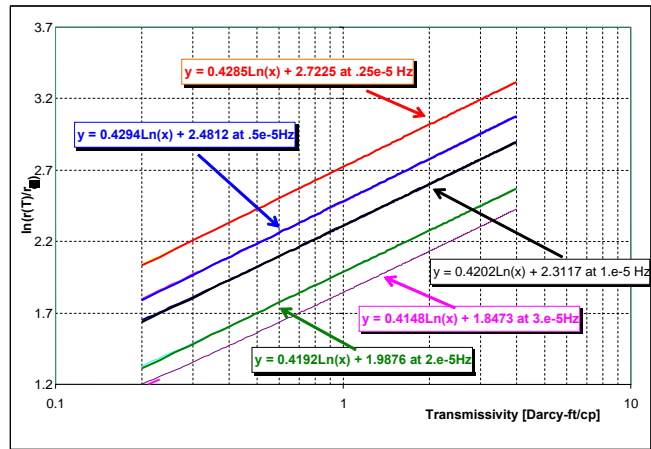

Fig. 7. Semilog plots of the radius of influence versus transmissivity at different frequencies, Like in Fig. 6, the scaling of the decay rate is consistently different from the anticipated square root of the transmissivity.

The synthetic data analysis suggests that frequency-domain analysis can be used for well performance evaluation by repeated tests like the ones shown in Fig. 5. The fluctuations in the pressures and rates are not large, so such a test can be performed as a part of regular field operations. The absolute value of the injectivity index involves both transmissivity and the radius of the zone of influence in a coupled manner. The history of the formation transmissivity and the influence zone radius estimates obtained on different time intervals, and comparison with the production and injection data from neighboring wells, can provide useful insights into the possible formation damage and water breakthrough. One can then promptly react by adjusting the controller target rate.

Use of InSAR subsidence images in field monitoring

The line-of-sight motion of land surface above the Lost Hills diatomite field is monitored every 24 days with use of the differential synthetic aperture radar interferograms (inSAR). The inSAR images are acquired and processed by Vexcel Corporation. The square voxel size is 20 m (67 ft). A recent, May-April, 2005, example - zoomed to encompass only parts of Sections 32 (west) and 33 (east) - is shown in **Fig. 12**. The downhole locations of the diatomite water injectors are shown as black squares and of the producers as open diamonds. Each injector-centered pattern covers roughly 3×3 voxels. The surface motion is very dynamic and has a significant elastic ("instantaneous") component. The red and yellow islands of uplift near the east flank become the blue islands of subsidence near the crest. The cumulative subsidence has been calculated by section and shown in **Fig 13**. Note that overall the subsidence has been arrested in Sections 32, 33 and 29, while it continues unabated in Section 4.

The oil and water production rates from well tests in April and May 2005, are shown in **Fig. 14** and **Fig. 15**. The point rates at the downhole well locations were interpolated linearly using the Delaunay triangulation. The result was then gridded using a triangular mesh, so that the hard well data were honored. A comparison of the latter two figures with Fig. 12 shows that that high oil production rate generally correlates with the arrested subsidence or uplift, while the high water production rate correlates with subsidence. This correlation is especially visible across the rectangular region in the south-central portion of the image, bordered from the west, north, and east by three faults.

The positive correlation of gross production with subsidence is clearly visible from the triangulated map in **Fig. 15**. It is interesting to note that the product of stroke frequency × stroke length × pump size[2] × fraction of time the pump is on (inch[3]/minute), see **Fig. 17,** is a good proxy for the gross production. Therefore, using the continuous pump-off controller data will be our preferred way of providing continuous production feedback to the injection controllers.
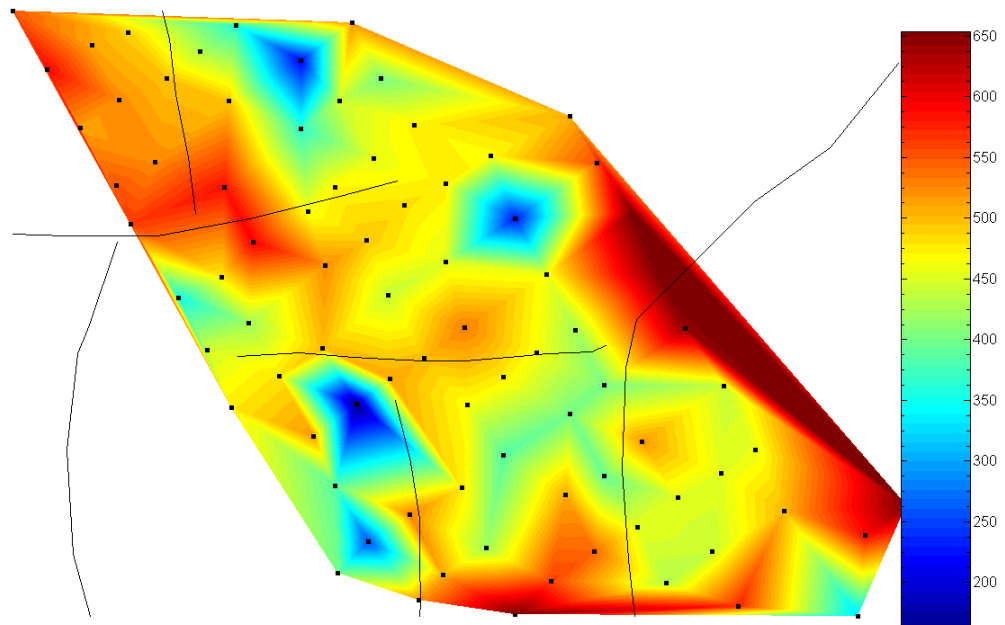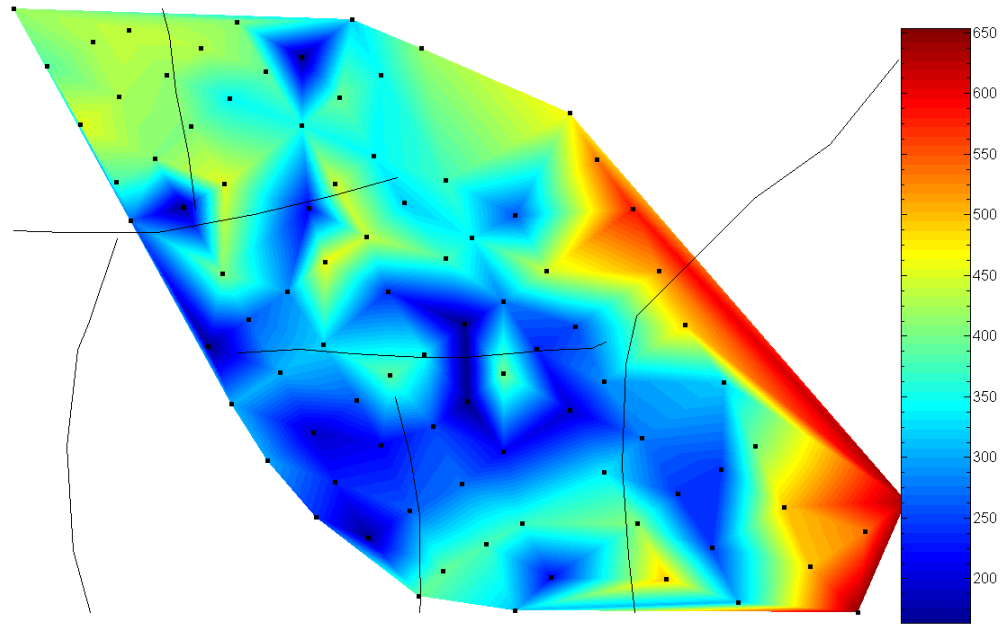
Fig. 8. Section 32 slope analysis reservoir pressure estimates for short- (the top map) and long-strings (the bottom map) of the dual water injectors. Although the injection fluctuations were not spatially correlated, there is a good correlation with the pressures maps, Figures Fig. 10 and Fig. 11 below.
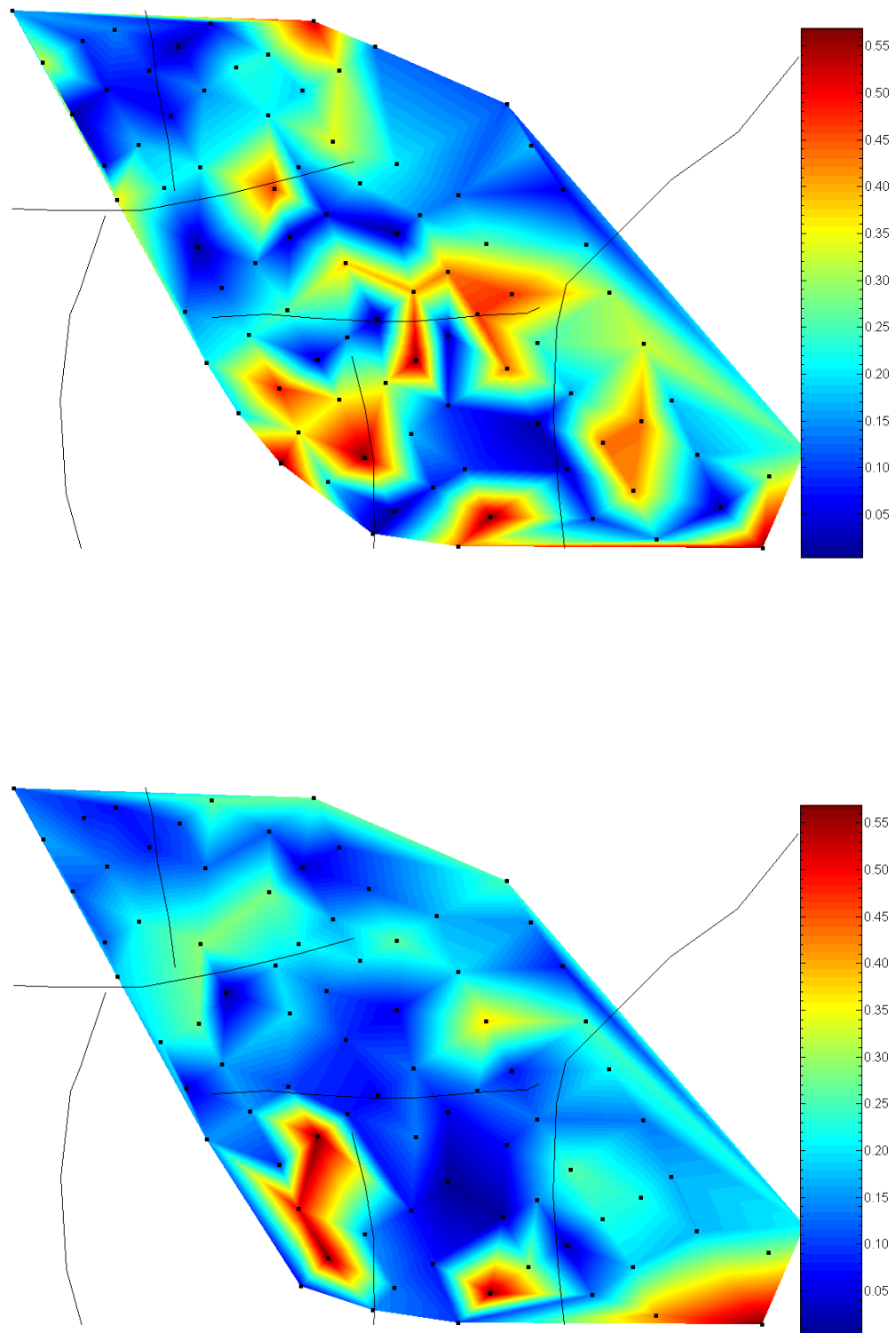
Fig. 9. Section 32 slope analysis intercepts in psi-day/bbl. Short string intercepts are displayed on the top map and the long-string intercepts on the bottom map. A larger intercept may mean either higher permeability of the formation near the wellbore, or a smaller injection fluctuations influence radius.
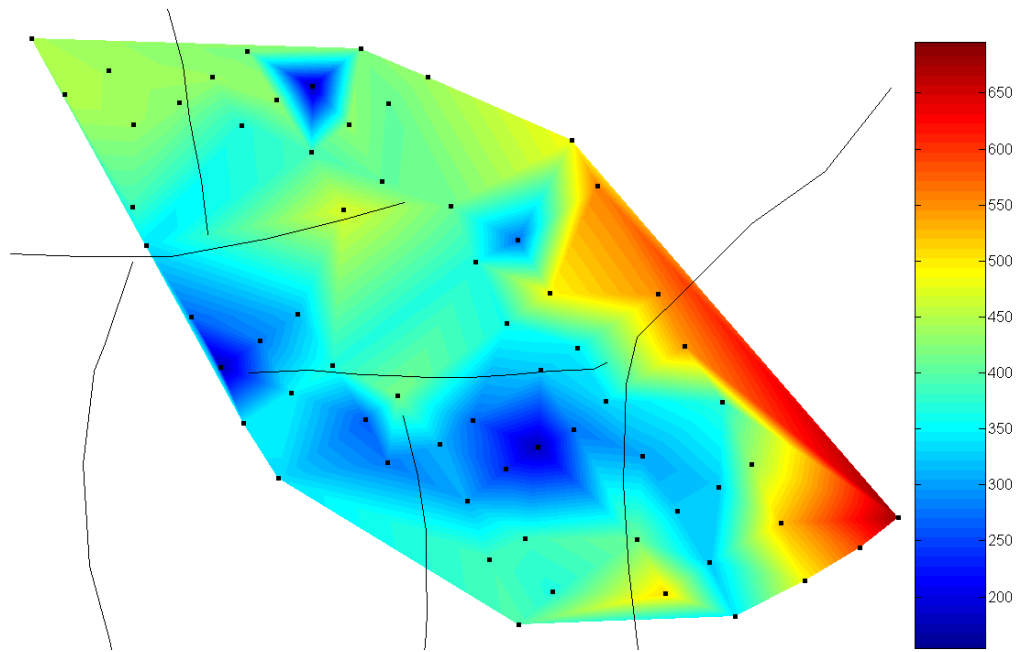
Fig. 10.The short-string injection pressure map in Section 32. The wellhead pressures are mapped for wells injecting at the similar rates. The red-color area to the north-east is apparently a low-permeability zone of the reservoir.
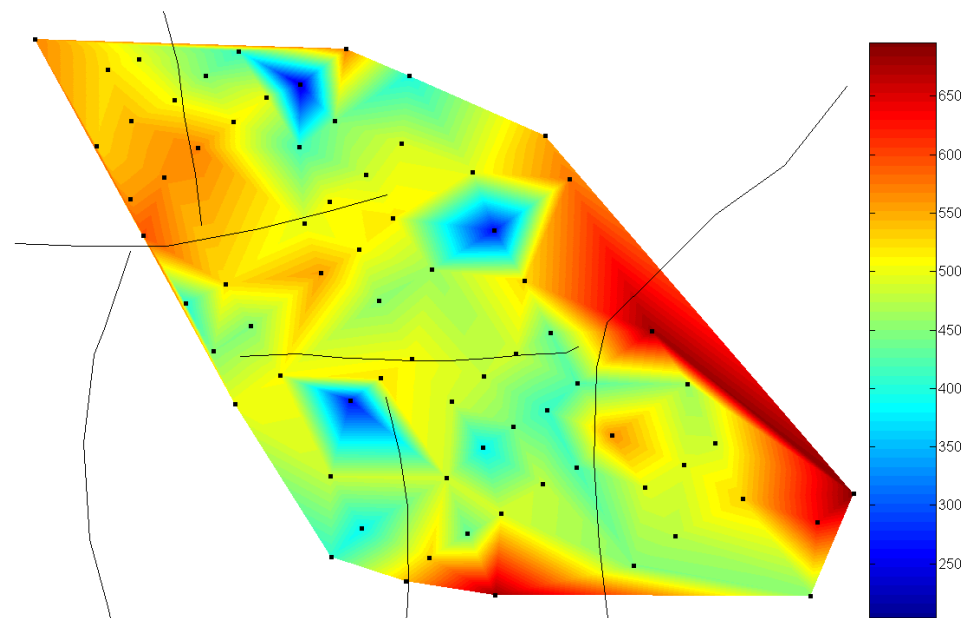

Fig. 11. Pressures map analogous to the one displayed in Fig. 10, but for the long strings. The pressures are higher than in Fig. 10; however, the low-permeability region to the north-east is also noticeable.
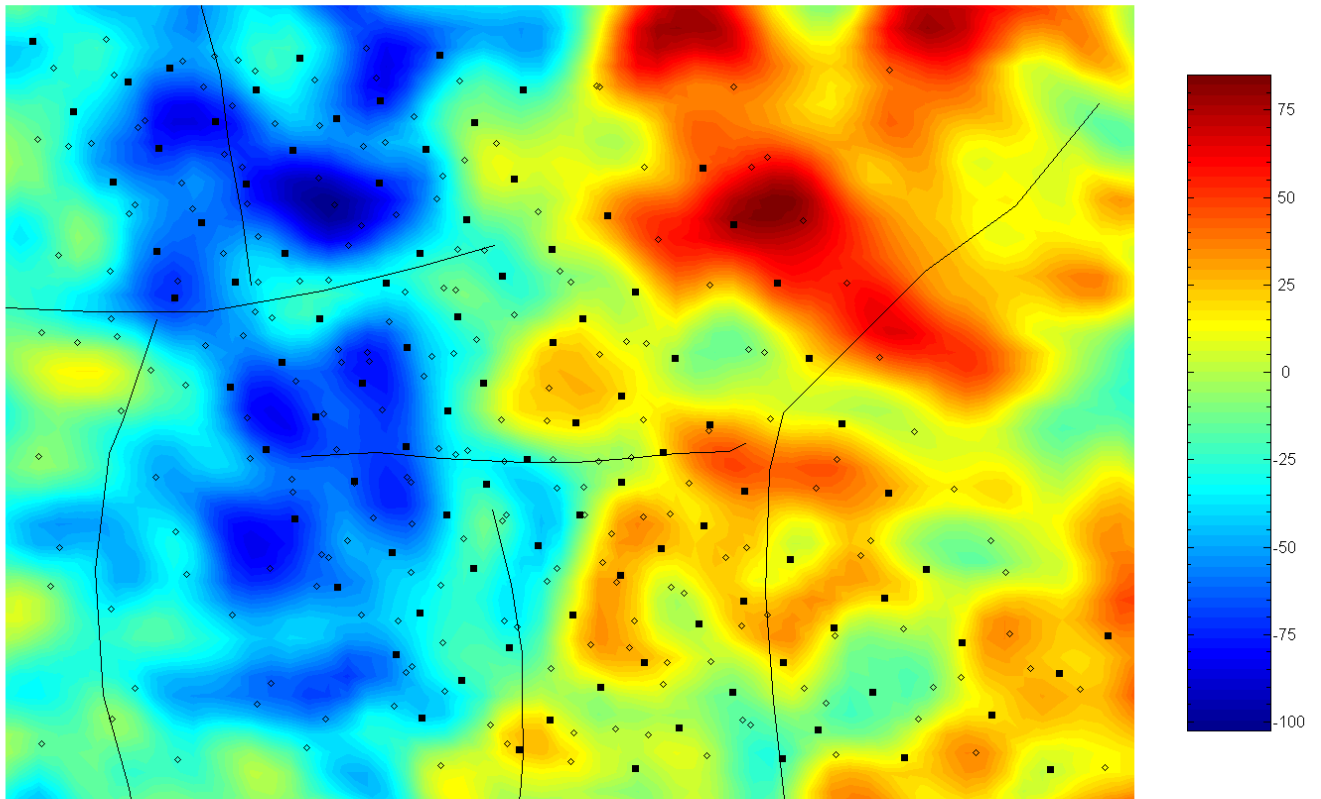
Fig. 12. The differential InSAR image of the line-of-sight surface displacement in the Lost Hills diatomite Sections 32 and 33. The InSAR images have been acquired and processed by Vexcel Corp. The time interval is May-April, 2005. The positive displacement values in mm/year reflect surface uplift, and the negative values subsidence. The black lines are traces of the major faults at the top of the diatomite. The downhole locations of the water injectors are shown as squares and of the producers as diamonds.
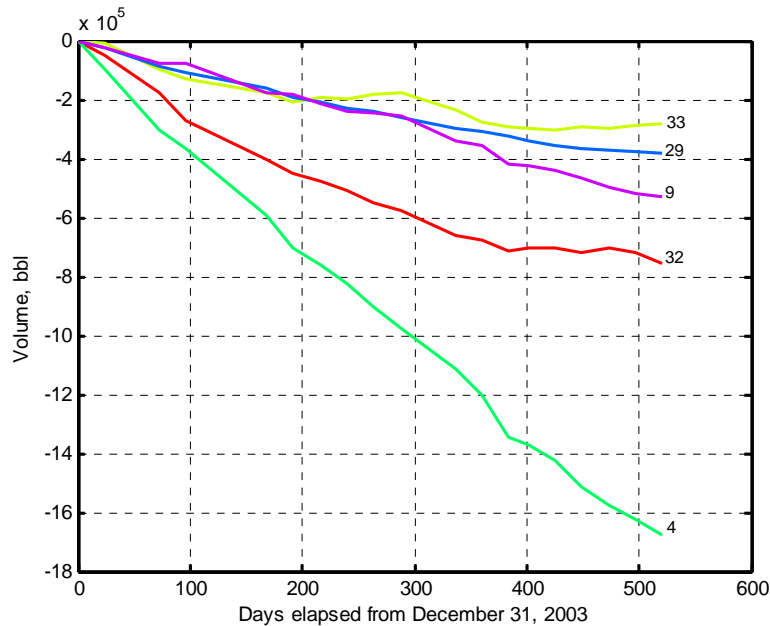
Fig 13. Surface subsidence in Lost Hills by section. Note the differences between Section 4 and 32 and 33.

Fig. 14. Triangulation of oil production (bopd) from well tests in April-May 2005. Note that the high oil production rate in the lower right portion of the image correlates with uplift. The upper left portion of the image suggests compaction drive.
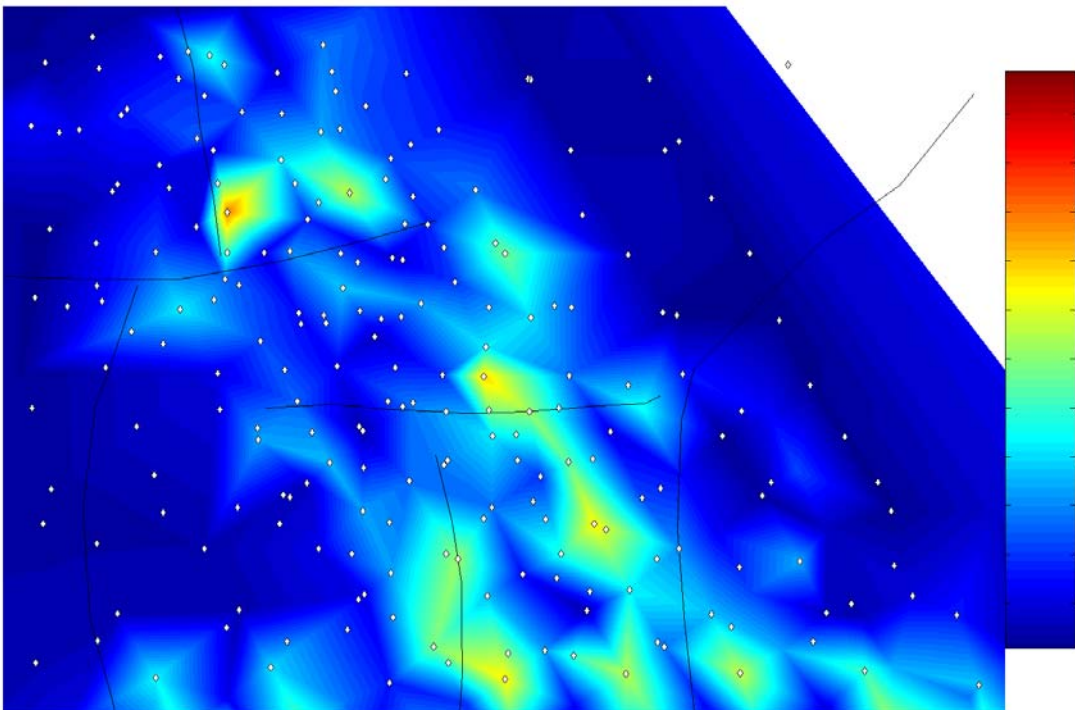
Fig. 15. Triangulation of water production (bwpd) from well tests in April-May 2005. Note that high water production rate in the center correlates well with subsidence.
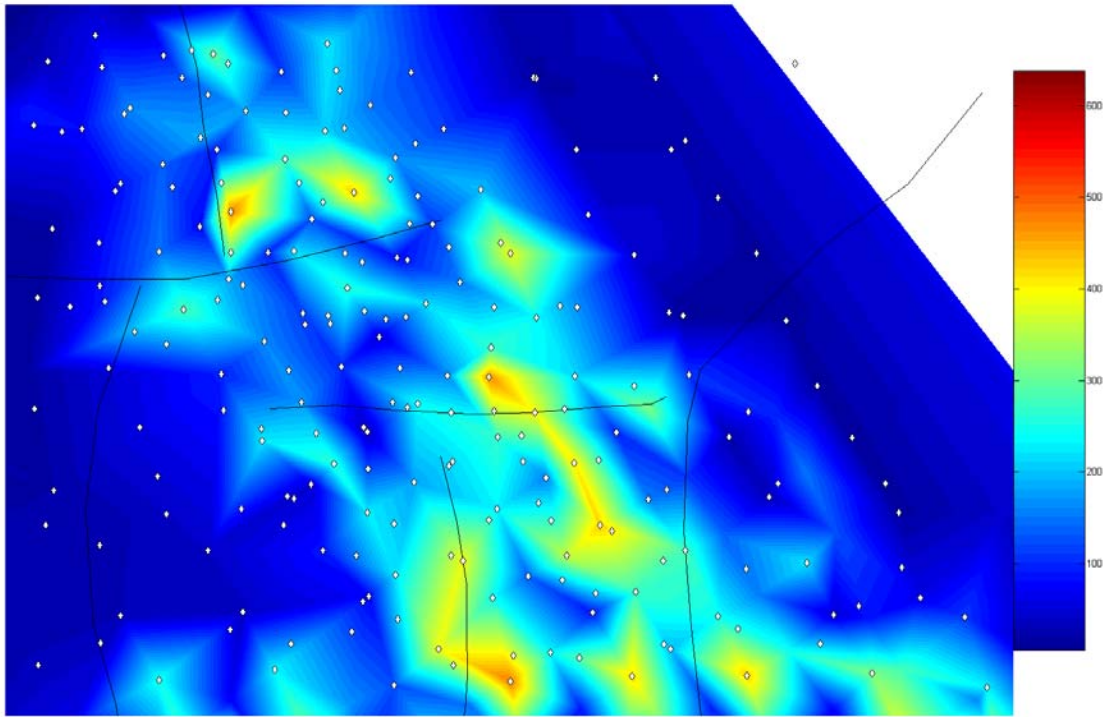
Fig. 16. Triangulation of gross production (bpd) from well tests in April-May 2005.
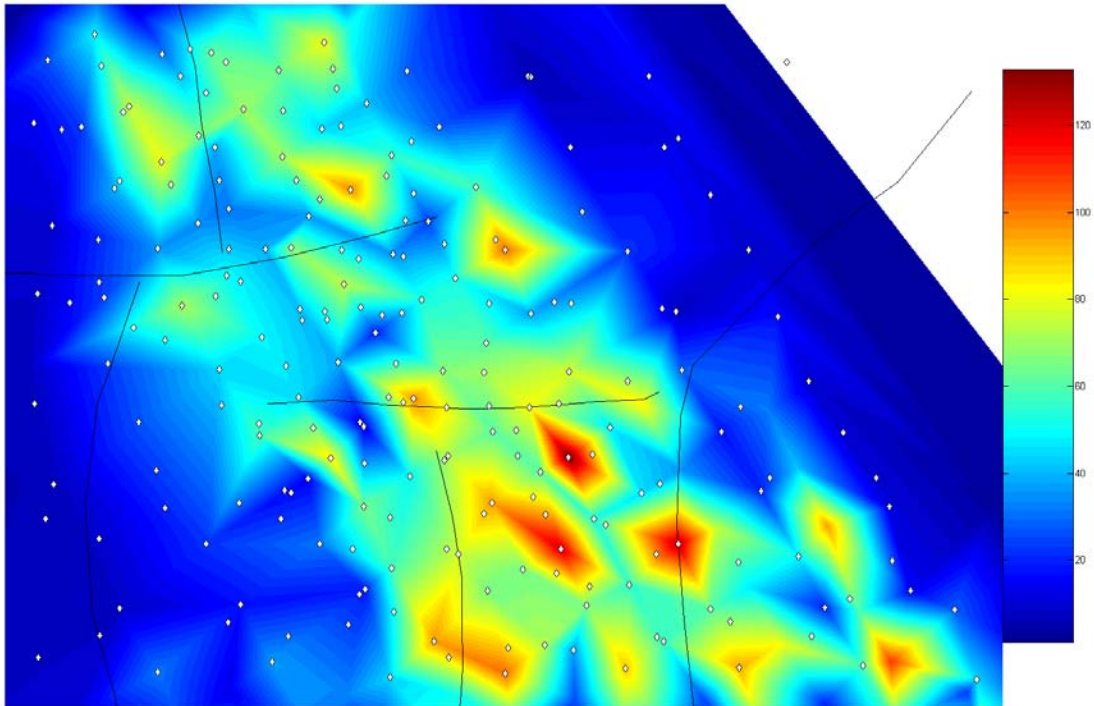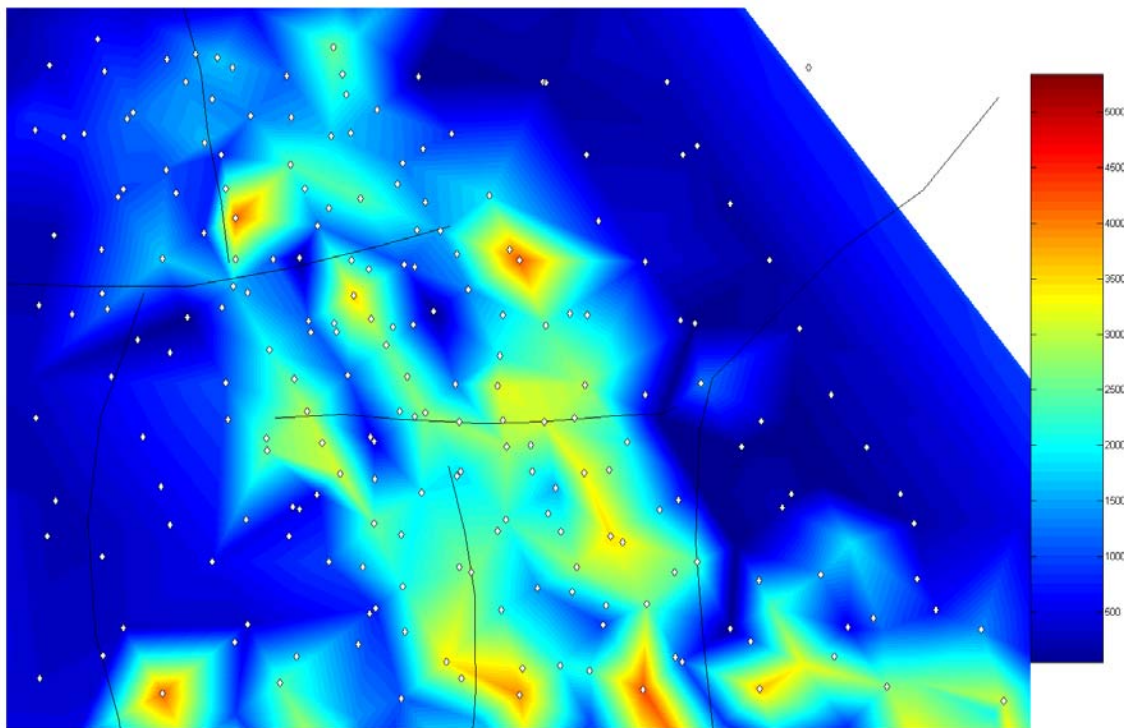

Fig. 17. Triangulation of pump utilization (inch^3/minute) from well tests in April-May 2005. Note the strict similarity to the gross production image above. Therefore, pump-off controller data can be used as a continuous proxy for the discrete well tests.

Conclusions

Waterflood automation at a field scale is a complex coupled problem. The input data are acquired from individual injection wells as time series of injection pressures and rates; from individual producers, as well test data and time series of pump stroke lengths. A combination of the Hall plot, slope analysis, transient test and frequency-domain calculations is used for the automatic and off-line monitoring of individual well performance. The satellite differential InSAR images provide valuable global information about surface subsidence and the formation damage, which is then fed back to the injection controllers. Some data are processed in automatic mode and some require input from qualified personnel. The automatic control loop is based on the principles of dynamic adaptive control. The nature of the fluid-rock interactions in a waterflood in soft rock requires a mixed open-loop-feedback control mode, in which the computed set points are generated and applied in a cyclic manner. Each control cycle concludes by updating the model parameters and control based on the information acquired as time series. This comprehensive field surveillance/control strategy is being implemented at the Lost Hills diatomite field, CA, USA.

Appendix A. The Hall plot and slope analyses

Transient fluid flow in a homogeneous, vertically-confined horizontal reservoir in cylindrical coordinates is characterized by the following equation

$$\frac{\partial^2 p}{\partial r^2} + \frac{1}{r}\frac{\partial p}{\partial r} + \frac{1}{r^2}\frac{\partial^2 p}{\partial \psi^2} = \frac{1}{D}\frac{\partial p}{\partial t} \qquad (1)$$

where r and ψ are the polar coordinates centered at the well, t is time, $p(t,r,\psi)$ is the fluid pressure, and D is the hydraulic diffusivity

$$D = \frac{k}{\mu c \phi} \qquad (2)$$

In the latter, c is the total compressibility of the fluid-saturated reservoir rock, k and ϕ are the rock permeability and porosity and μ is the fluid viscosity. By the nature of the polar coordinate system, all functions in Eq. (1) are periodical with respect to ψ. Integration of both sides of Eq. (1) in ψ and division by 2π eliminates the last term on the left-hand side and replaces the point values of pressures with the mean values. Therefore, in what follows, the pressures at a given radius are the mean pressures over the circle of this radius. Then, the steady state flow equation is

$$\frac{\partial^2 p}{\partial r^2} + \frac{1}{r}\frac{\partial p}{\partial r} = 0 \qquad (3)$$

The pressure distribution at a given injection rate Q is given by

$$p(r) = p_e + \frac{\mu}{2\pi kH}\ln\frac{r_e}{r}Q \qquad (4)$$

Here H is the thickness of the injection zone, p_e is the injection pressure at the external perimeter of the zone of injection, and

r_e is the radius of this zone. In steady-state flow, where the time scale of the transient processes is much smaller than that of the time of observation, Eq. (4) holds true even if the pressures and rates are functions of time. The idea of Hall analysis[14] is that if the injection interval transmissivity $T=kH/\mu$ and the radius of injection zone r_e do not significantly change over the time interval of observations, then the plot of the integral

$$\Pi(t) = \int_{t_0}^{t} \left(p_w(\tau) - p_e\right) d\tau \qquad (5)$$

versus the cumulative injection

$$V(t) = \int_{t_0}^{t} Q(\tau) d\tau \qquad (6)$$

must be a straight line. Thus, a deviation from a straight line should signify alterations of the formation properties. The simplicity of this injection performance monitoring method is offset by the necessity to determine the ambient reservoir pressure p_e. Silin et al.[15] have demonstrated that if an incorrect estimate of p_e is used in Hall's analysis, then the change of slope may occur when no transmissivity modifications happen and, conversely, the changing injectivity can be hidden.
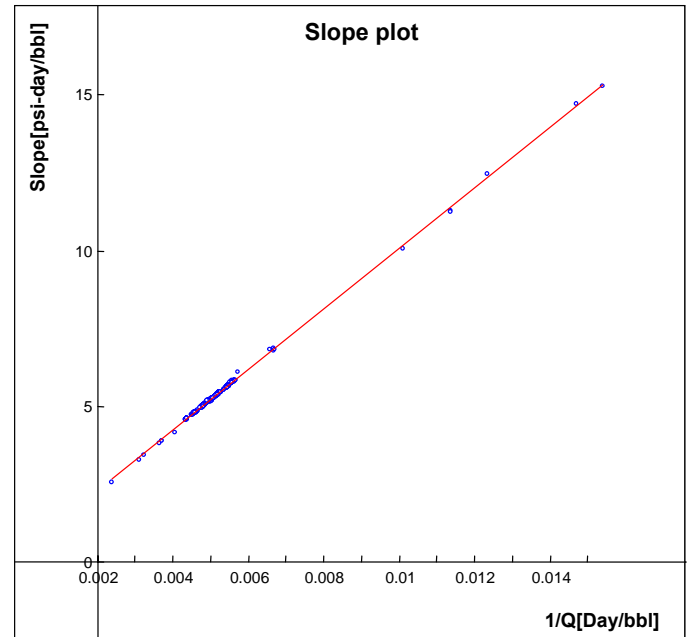
Fig. 18. An example of slope analysis: the points computed from data are aligned along a straight line (bottom). The rates, Fig. 2, have noticeable fluctuations. The slope is estimated at 971 psi and the intercept is 0.35 psi-day/bbl.

To correctly interpret the Hall plot, a novel "slope analysis" has been proposed in Ref.[15]. The idea was to use the inevitable fluctuations in pressure and rate to estimate p_e. If both sides of Eq. (4) are divided by Q,

$$\frac{p_w}{Q} = \frac{p_e}{Q} + \frac{\mu}{2\pi kH}\ln\frac{r_e}{r} \qquad (7)$$

then p_w/Q is a linear function of $1/Q$, and the slope of the plot of this function is the reservoir pressure at the perimeter of the injection zone, see **Fig. 18**.

The latter concept needs an additional comment. The ambient pressure estimate furnished by slope analysis is coupled with the estimate of the intercept of the straight line defined by Eq. (7). The rate and pressure fluctuations may happen on different time scales. The portion of the reservoir affected by these fluctuations depends on this time scale. High-frequency fluctuations affect a smaller domain than the low-frequency fluctuations. Note that by the nature of the processes and the way the data are collected, the high frequency in this context means a tiny fraction of 1 Hz, and is far below the seismic low-frequency range. A plot of the slope and intercept estimates obtained for the same well from different data intervals is presented in **Fig. 19**. The linearity of the plot confirms the logarithmic scaling of the reservoir pressure decay against the distance to the wellbore in steady-state injection.
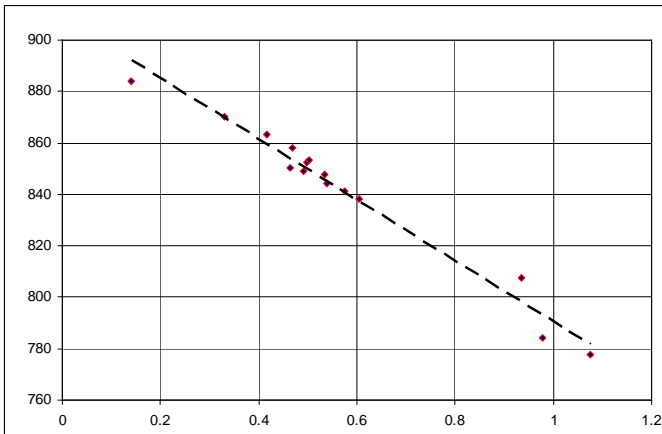

Fig. 19. The slope (vertical axis, in psi) versus the intercept (psi-day/bbl) measured at the same well, but on different data sets are aligned along a straight line. The linear fit describes the logarithmic reservoir pressure decay with the distance from the wellbore, *cf.* Eq. (7).

Appendix B. Frequency-domain analysis of the injection pressure – injection rate ratio

Although normally the injected fluid has a constant composition, its pressure and rate are not exactly constant. The steady-state flow is accompanied by relatively small fluctuations. When the driving force, the injection pressure, deviates from its mean value, the injection rate reacts by its own deviation from its mean value. Such deviations are used in the slope analysis to estimate the local mean reservoir pressure and correct Hall's method. Here we analyze these fluctuations by mapping them in the frequency domain. We use the same notations as in Appendix A.

We use the radial flow equation with the homogeneous fluid and reservoir properties in the dimensionless form as in Ref. 10:

$$\frac{\partial^2 p}{\partial r^2} + \frac{1}{r}\frac{\partial p}{\partial r} = \frac{1}{D}\frac{\partial p}{\partial t} \tag{8}$$

Here p is the reservoir pressure, r is the distance from the wellbore, and t is time. Coefficient D is the hydraulic diffusivity (2). We seek a solution in the form

$$p(t,r) = e^{i\omega t}\overline{p}(\omega,r) \tag{9}$$

which is equivalent to solving Equation (8) in frequency domain. Here i is the square root of -1, ω is the angular frequency and $\overline{p}$ is the pressure amplitude, a function yet to be determined.

The pressure amplitude $\overline{p}(\omega,r)$ as a function of r, is a Bessel function of zeroth order satisfying the equation:

$$\frac{\partial^2 \overline{p}}{\partial r^2} + \frac{1}{r}\frac{\partial \overline{p}}{\partial r} - i\frac{\omega}{D}\overline{p} = 0 \tag{10}$$

A solution to this equation is a combination of Bessel functions of the first and second kind[20]. In radial flow model, only the zero-order functions produce sensible solutions[21]. After slight modifications, standard calculations yield a solution expressed through a Bessel function of the first kind in the form of power series

$$\varphi(r) = 1 + i\frac{\omega}{D}\left(\frac{r}{2}\right)^2 + \frac{\omega^2}{D^2(2!)^2}\left(\frac{r}{2}\right)^4 + \ldots \tag{11}$$

Here $\varphi(r) = J_0\left(e^{i\frac{\pi}{4}}\sqrt{\frac{\omega}{D}}\,r\right)$. Note that the coefficient $e^{i\frac{\pi}{4}}$ is a complex number with both real and imaginary parts not equal to zero. We focus only on the low-frequency signals in a close neighborhood of the wellbore, $\varepsilon = \frac{\omega}{D}r^2$ is a small parameter, so we can truncate the series (11). Fro example, assume the permeability of the order of 1 Darcy, the porosity 30%, the fluid viscosity 1 cp, and the total compressibility of the order of 10^{-9} Pa^{-1}. Then, for r_c=50 ft, and the periodicity of fluctuations of the order of 10 hours, parameter ε is of the order of 0.01.

The general solution to Eq. (10), given by

$$\overline{p} = \varphi_0(r)\left(\int_r^{r_c}\frac{C_1}{\xi\varphi_0^2(\xi)}d\xi + C_2\right) \tag{12}$$

has a logarithmic singularity as $r/r_c \to 0$. Here r_c is some characteristic distance from the wellbore, intermediate between the wellbore radius r_w and the influence domain radius, r_e. Such choice of distance scaling makes possible asymptotic analysis of the pressure distribution assuming that both r_w/r_c and r_c/r_e are small parameters. The constant coefficients C_1 and C_2 are determined by the boundary conditions. Note that both C_1 and C_2 are complex functions of frequency ω. An appropriate combination of C_1 and C_2 yields a modified Bessel function of the second kind K_0, exponentially vanishing at infinity for real variables, Ref. 20. Due to this property, K_0 is normally used in the frequency-domain analysis of Eq. (8), Ref. 22.

The flow rate corresponding to the pressure distribution (9) has the form $Q = e^{i\omega t}\overline{Q}(\omega,r)$, where the amplitude $\overline{Q}$ is calculated from $\overline{p}$ by Darcy's law,

$$\overline{Q}(\omega,r) = -2\pi rH\frac{k}{\mu}\frac{\partial \overline{p}(\omega,r)}{\partial r} \tag{13}$$

Here H, as in Appendix A, is the thickness of the injection interval. We also adopt the convention that for injection the flow rate is positive. By virtue of Eq. (11), $\dfrac{\partial J_0(r)}{\partial r} = O(r)$. Hence, coefficient C_1 is different from zero if the flow rate amplitude near the wellbore is not equal to zero.

Substitution of expansion (11) into Equation (12) yields

$$\bar{p} = C_1\left(1+i\frac{\omega}{D}\left(\frac{r}{2}\right)^2\right)\left(\int_r^{r_c}\frac{1}{\xi\left(1+i\frac{\omega}{D}\left(\frac{\xi}{2}\right)^2+\ldots\right)}d\xi\right) \quad (14)$$
$$+C_2\left(1+i\frac{\omega}{D}\left(\frac{r}{2}\right)^2\right)+\ldots$$

where we have dropped the terms of higher order. Note that

$$\frac{1}{\xi\left(1+i\frac{\omega}{D}\left(\frac{\xi}{2}\right)^2+\ldots\right)} = \frac{1}{\xi} - \frac{i\frac{\omega}{D}\left(\frac{1}{2}\right)^2\xi+\ldots}{\left(1+i\frac{\omega}{D}\left(\frac{\xi}{2}\right)^2+\ldots\right)} \quad (15)$$

Hence the principal term in the integral is $\ln\dfrac{r_c}{r}$, and

$$\bar{p} = C_1\left(1+i\frac{\omega}{D}\left(\frac{r}{2}\right)^2\right)\ln\frac{r_c}{r} + C_2\left(1+i\frac{\omega}{D}\left(\frac{r}{2}\right)^2\right)+\ldots \quad (16)$$

Clearly, the additive terms in Equations (16) can be combined by the introduction of some characteristic radial distance $r(\omega)$:

$$\bar{p} = C_1\left(1+i\frac{\omega}{D}\left(\frac{r}{2}\right)^2\right)\ln\frac{r(\omega)}{r}+\ldots \quad (17)$$

The physical sense of this distance is clear: at $r=r(\omega)$ the pressure amplitude vanishes up to the terms of higher order. Substitution of the last estimate into Equation (13) yields

$$\bar{Q} = C_1 2\pi H\frac{k}{\mu}\left[\left(1+i\frac{\omega}{D}\left(\frac{r}{2}\right)^2\right)-i\frac{\omega r^2}{2D}\ln\frac{r(\omega)}{r}\right]+\ldots \quad (18)$$

The comparison of zero-order terms yields the usual steady-state flow equation

$$\bar{p}(\omega,r) = \frac{\mu}{2\pi kH}\ln\frac{r(\omega)}{r}\bar{Q} \quad (19)$$

cf. Eqs. (4). A more delicate result is obtained if the next asymptotic terms of $\bar{p}$ and $\bar{Q}$ are compared. Assuming that $\ln\dfrac{r(\omega)}{r} \gg 1$, one infers

$$\left|\frac{\bar{p}(\omega,r)-\bar{p}(\omega,0)}{\bar{Q}(\omega,r)-\bar{Q}(\omega,0)}\right| = \frac{\mu}{4\pi kH}+\ldots \quad (20)$$

In other words, the ratio of the next asymptotic terms is inversely proportional to the transmissivity factor. In particular, the right-hand side of Eq. (20) is independent of the frequency and has a nonzero limit as r→0. At sufficiently low frequency fluctuations, Eq. (20) could be used if data from a pressure observation well were available.

Acknowledgments

Nomenclature

c = fluid/formation compressibility, psi^{-1}
D = hydraulic diffusivity, $\text{m}^2\text{/s}$
H = reservoir thickness, ft
J_0 = Bessel function of the first kind and zero order
K_0 = modified Bessel function of the second kind and zero order
k = absolute rock permeability near the wellbore, Darcy
p_w = wellbore pressure, psi
p_e = average pressure in the formation, psi
p_{w0} = wellbore pressure at the beginning of data interval, psi
r_e = influence zone radius, ft
r_{wb} = wellbore radius, ft
r_w = effective wellbore radius, ft
Q = injection rate, bbl/day
s = skin factor, dimensionless
T = transmissivity, Darcy-ft/cp
ϕ = porosity, dimensionless
μ = fluid viscosity, cp
ω = angular frequency, Hz

SI Metric Conversion Factors

Darcy	× 9.869	E-13 = m^2
bbl	× 1.589 873	E-01 = m^3
cp	× 1.0*	E-03 = Pa s
bbl/day	× 6.62	E-03 = $\text{m}^3\text{/s}$
ft	× 3.048*	E-01 = m
ft^3	× 2.831 685	E-02 = m^3
in	× 2.54*	E+00 = cm
psi	× 6.894 757	E+00 = kPa

References

[1] Talash, A.W., "An Overview of Waterflood Surveillance and Monitoring," Journal of Petroleum Technology, 1988 (December): p. 1539-1543.

[2] Brink, J.L., T.W. Patzek, D.B. Silin, and E.J. Fielding. Lost Hills Field Trial - Incorporating New Technology for Reservoir Management. in SPE Annual Technical Conference and Exhibition. 2002. San Antonio, Texas: SPE.

[3] Patzek, T.W., D.B. Silin, and E. Fielding. Use of Satellite Radar Images in Surveillance and Control of Two Giant Oilfields in California. SPE71610. in 2001 SPE Annual Technical Conference and Exhibition. 2001. New Orleans, LA: SPE.

[4] Patzek, T.W. Surveillance of South Belridge Diatomite SPE 24040 SPE Western Regional Meeting, 30 March-1 April, Bakersfield, California, 1992

[5] Barenblatt, G. I., T.W. Patzek, V.M. Prostokishin, and D.B. Silin, Oil Deposits in Diatomites: A New Challenge for Subterranean Mechanics SPE 75320 SPE/DOE Improved Oil Recovery Symposium, 13-17 April, Tulsa, Oklahoma 2002

[6] Silin, D.B. and T.W. Patzek, "Water injection into a low-permeability rock - 2: Control model," Transport in Porous Media, 2001a. 43(3): p. 557-580.

[7] Silin, D.B. and T.W. Patzek, "Control model of water injection into a layered formation," SPE Journal, 2001b. 6(3): p. 253-261.

[8] Muskat, M. Physical principles of oil production. McGraw-Hill Book Co. 1949.

[9] Matthews, C.S. and D.G. Russell, Pressure Buildup and Flow Tests in Wells. 1967, New York, NY: SPE of AIME.

[10] Earlougher, R.C., Advances in Well Test Analysis. Monograph Series. Vol. 5. 1977, New York: Society of Petroleum Engineers.

[11] Silin, D.B. and C.-F. Tsang, "Estimation of Formation Hydraulic Properties Accounting for Pre-Test Injection or Production Operations,". Journal of Hydrology, 2002. 265(1): p. 1-14.

[12] Silin, D.B. and C.-F. Tsang, "A well-test analysis method accounting for pre-test operations," SPE Journal, 2003 (March): p. 22-31.

[13] Patzek, T. W. and Silin, D. B. Control of Fluid Injection into a Low-Permeability Rock - 1. Hydrofracture Growth. Transport in Porous Media, 2001, 43, No. 3, 537-555.

[14] Hall, H.N., "How to Analyze Waterflood Injection Well Performance,". World Oil, 1963 (October): p. 128-130.

[15] Silin, D.B., R. Holtzman, T.W. Patzek, and J.L. Brink. Monitoring Waterflood Operations: Hall's Method Revisited SPE 93879 2005 SPE Western Regional Meeting Irvine, CA, U.S.A., 30 March – 1 April 2005.

[16] Johnson, C. R., R. A. Greencorn, and E. G. Woods. A New Method for Describing Reservoir Flow Properties between Wells. Journal of Petroleum Technology, 1966, December, p. 1599-1604

[17] Streltsova, T. D. Well testing in heterogeneous formations. Wiley, New York, 1988.

[18] Raghavan, R. Well Test Analysis. Prentice Hall, N. Y., 1993

[19] Press, W. H.; Flannery, B. P.; Teukolsky, S. A.; and Vetterling, W. T. Numerical Recipes in C: The Art of Scientific Computing, 2nd ed. Cambridge University Press, Cambridge, England: 1992.

[20] Tikhonov, A.N., and A. A. Samarskii. Equations of Mathematical Physics. New York, Macmillan, 1963.

[21] Barenblatt, G. I., V. M. Entov, and V. M. Ryzhik, Theory of Fluid Flows through Natural Rocks, Kluwer Academic Publishers, Dordrecht, 1990.

[22] Rosa, A. J., and R. N. Horne. Reservoir Description by Well Test Analysis Using Cyclic Flow Rate Variation. SPE Paper 22698 Presented at 66th ATCE, Dallas, TX, October 6-9, 1991